Processing model for tungsten powders and extension to nanoscale size range

Randall M. German*[1], J. Ma[2], X. Wang[2] and E. Olevsky[2]

Nanoscale tungsten powders promise access to very hard, strong and wear resistant materials via the press–sinter route. A small particle size changes the response during sintering, requiring lower temperatures and shorter times to attain dense but small grain size structures. On the other hand, oxide reduction and impurity evaporation favour high sintering temperatures and long hold times. Accordingly, press–sinter processing encounters conflicting constraints when applied to small particles. Presented here is an analysis of press–sinter tungsten particle processing to isolate conditions that balance the temperature and size dependent effects. The calculations are pinned by existing data. Opportunities are identified for new consolidation approaches to deliver a small grain size in a full density structure.

Keywords: Tungsten, Nanoscale, Sintering, Compaction, Powder Metallurgy

Introduction

Tungsten, tungsten alloys and tungsten compounds occupy unique positions in materials science. Most uses derive from combinations of the high density, hardness, melting temperature, elastic modulus, radiation opacity, and thermal–electrical conductivity in conjunction with low thermal expansion. Tungsten was one of the first metallic nanoscale powders.[1] Prior reports give data on the processing of nanoscale W,[1–6] W–Cu,[7–13] W–Ni–Fe,[14] W–Cu–Al–Ni,[15] W–Y and W–Y_2O_3.[16] Strength, hardness, and wear resistance will improve with a small grain size. For example, the Hall–Petch effect (hardness increases in proportion to the inverse square root of grain size) suggests significant gains if nanoscale powders could be consolidated to full density with a small grain size. In spite of nanoscale powder availability, success has been difficult because these powders undergo rapid microstructure coarsening when sintered.[4,10,12–19] Consequently, novel but expensive consolidation routes are used to lower the densification temperature as a means to reduce grain growth.[4,20,21] In traditional press–sinter processing, temperature dependent reactions are embedded in the high temperature heating cycle, but low temperature consolidation tends to trap the contaminants. Thus, the conflicts between size dependent events, such as a low sintering temperature, and temperature dependent events, such as oxide reduction, create imbalances that often result in sintered properties below expectations.

Prior research has generated press–sinter data for tungsten powders over a broad particle size range. Data exists for particle sizes ranging from 20 nm to 18 μm and sintering temperatures up to 2700°C.[1,3,5,6,20–44] This body of knowledge provides a basis for predicting property levels, processing effects, and opportunities for tungsten based materials at the nanoscale. These data are combined with processing models in a form that handles micrometre to nanometre particle sizes. From this base predictions are made for product properties as functions of the particle size and processing conditions. When the earlier efforts employed nanoscale powders, almost always traditional processing cycles were applied, with little reported property gain.

Hence, with the novel and new powders comes a need to identify novel processing routes to produce improved materials and properties. Although some of the processing attributes of tungsten powders scale with particle size, there are other aspects that encounter temperature constraints. Nanoscale tungsten needs to be assessed in the context of this balance. Modelling, such as performed here, provides a means to identify processing options customised to nanoscale tungsten based materials. The model is constructed to predict performance parameters including hardness, ductile–brittle transition temperature, strength, and wear resistance from the processing and initial powder characteristics. Success here provides a basis for analysing other materials and processing objectives. Based on this model, future experimental studies with nanoscale powders based on high compaction pressures, low sintering temperatures, and short sintering times seem most justified.

[1]Mechanical Engineering Centre for Advanced Vehicular Systems, PO Box 5404, Mississippi State University, MS 39762–5405, USA
[2]Mechanical Engineering Department, San Diego State University, 5500 Campanile Drive, San Diego, CA 92182–1323, USA

*Corresponding author, email german@cavs.msstate.edu

Modelling

Particle packing

Small particles have inhibited packing owing to the high surface area and interparticle friction.[45] The existing

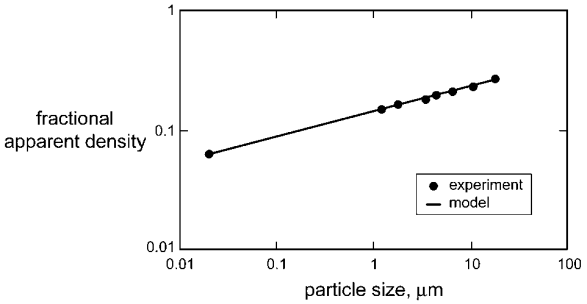

1 Log–log plot of fractional apparent density versus particle size, showing agreement between model and experimental results for deagglomerated tungsten

tungsten packing data are fit as follows

$$\log(\rho_A) = \log(\rho_0) + a \log D \quad (1)$$

where ρ_A is the fractional apparent density, ρ_O is the fractional packing density at 1 μm, a is a constant, and D is the median particle size in μm. Large spheres pack to 0·6 apparent density, but colloidal particles pack to densities as low as 0·05. For deagglomerated tungsten powder with a prismatic particle shape, ρ_O=0·143 and a=1/5. These constants were derived using packing data taken from powders in the range of 20 nm–18 μm (Ref. 5). The fit is illustrated in Fig. 1.

Compaction

Traditionally, powder is loaded at the apparent density into hard tooling for compaction. A polymer might be added to lubricate the tooling. Pressure is applied to the powder to increase density via rearrangement and plastic deformation at the particle contacts. The density after compaction is termed the green density. Powders exhibit a declining rate of densification with increasing pressure as the powder work hardens to resist further densification. Hard particles are very resistant to compaction.[46] Typical compaction models rely on the apparent density as the zero pressure density, and include a means to account for particle rearrangement, deformation, and work hardening. For compaction pressures >50 MPa, these factors give the fractional green density ρ_G as a function of the compaction pressure P

$$\rho_G - \rho_A = 1 - \rho_A \exp\left(B - \frac{P}{C}\right) \quad (2)$$

where ρ_A is the fractional apparent density. The rearrangement term B for tungsten depends on the particle size and its packing

$$B = \frac{1{\cdot}545}{D^{1/7}} \quad (3)$$

where the particle size D is in μm, compaction pressure P is in MPa, and the constant C is 1650 MPa. The predicted density is limited to 100% for very high compaction pressures. Most of the experimental data for tungsten compaction were collected over the pressure range from 50 to 300 MPa (0·47–0·64 fractional density) and tend to have 1–2% scatter, so the precision of the constants in equations (2) and (3) is no better. For example, at 207 MPa the fractional green density for a 6·5 μm powder is 0·61 and equation (2) predicts 0·60, and for a 1·2 μm powder at the same pressure the measured fractional density is 0·55 and the predicted

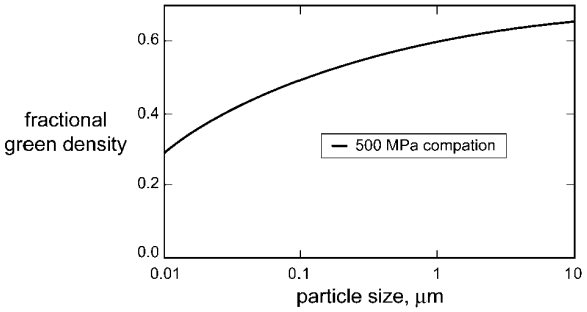

2 Model predicted fractional green density versus tungsten particle size for 500 MPa compaction pressure

value is 0·56. As a demonstration of equation (2), Fig. 2 plots the green density versus particle size down to 10 nm for a constant compaction pressure of 500 MPa.

The relationship between the compaction pressure and fractional green density can be determined from plasticity theory for porous bodies.[47] For isostatic compaction of porous materials

$$\sigma_r = \psi(1-\theta_G)^{1/2}\sigma_y \quad (4)$$

where σ_r is the radial stress, ψ is the normalised bulk modulus, θ_G is the green porosity of the powder compact, and σ_y is the yield stress of the fully dense powder material. The first invariant of a stress tensor (the hydrostatic pressure) for rigid die compaction is

$$P = \frac{1}{3}(\sigma_z + 2\sigma_r) \quad (5)$$

where σ_x is the axial stress. For isostatic pressing $\sigma_z = \sigma_r$. Therefore

$$P = \frac{1}{3}(\sigma_z + 2\sigma_r) = \sigma_r \quad (6)$$

from equations (4) and (6), we have

$$P = \psi(1-\theta_G)^{1/2}\sigma_y \quad (7)$$

hence

$$\psi = \frac{P}{(1-\theta_G)^{1/2}\sigma_y} = \frac{P}{(\rho_G)^{1/2}\sigma_y} \quad (8)$$

where $\rho_G = 1-\theta_G$ is the fractional green density of the compacted specimen. From equation (2), one can derive P as a function of C, B, ρ_G, and ρ_A as follows

$$\frac{1-(\rho_G-\rho_A)}{\rho_A} = \exp\left(B - \frac{P}{C}\right) \Rightarrow$$

$$B - \frac{P}{C} = \ln\left[\frac{1-(\rho_G-\rho_A)}{\rho_A}\right] \Rightarrow$$

$$P = C\left\{B - \ln\left[\frac{1-(\rho_G-\rho_A)}{\rho_A}\right]\right\} \quad (9)$$

combining equations (9) and (7), it can be concluded that

$$\psi = \frac{C}{(\rho_G)^{1/2}\sigma_y}\left\{B - \ln\left[\frac{1-(\rho_G-\rho_A)}{\rho_A}\right]\right\} \quad (10)$$

for the compaction of porous nanoscale materials in a rigid die[48]

$$\sigma_z = \frac{\sigma_y}{W}\left[\varphi\dot{\varepsilon}_z + \left(\psi - \frac{1}{3}\varphi\right)(\dot{\varepsilon}_z + 2\dot{\varepsilon}_r)\right] \quad (11)$$

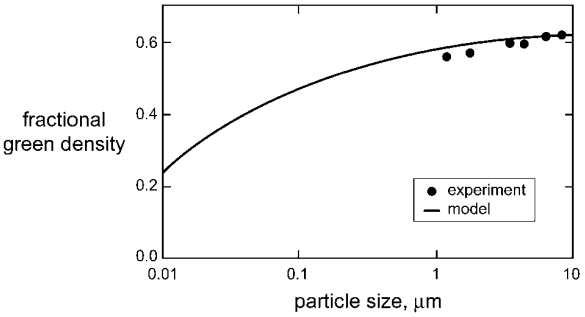

3 Comparison of modelling and experimental results for compaction of tungsten powders under 240 MPa stress

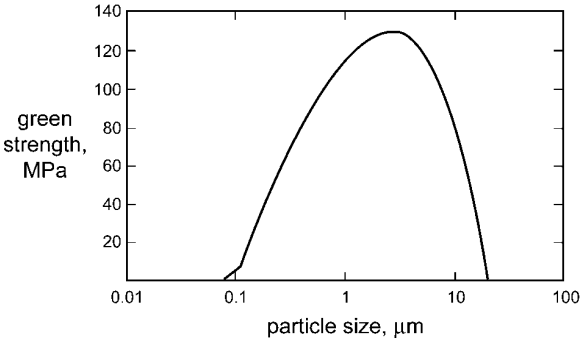

4 Predicted green strength from various tungsten particles compacted at 500 MPa

in this case $\dot{\varepsilon}_r = 0$. Therefore, equation (11) can be rewritten as follows

$$\sigma_z = \frac{\sigma_y}{W}\left[\varphi\dot{\varepsilon}_z + \left(\psi - \frac{1}{3}\varphi\right)\dot{\varepsilon}_z\right] \Rightarrow$$
$$\sigma_z = \frac{\sigma_y}{W}\dot{\varepsilon}_z\left(\psi + \frac{2}{3}\varphi\right) \quad (12)$$

where the equivalent effective strain rate W

$$W = \frac{1}{\rho_G^{1/2}}\left(\varphi\gamma^2 + \psi\dot{e}^2\right)^{1/2} \quad (13)$$

and $\dot{\gamma} = \left(\frac{2}{3}\right)^{1/2}|\dot{\varepsilon}_z - \dot{\varepsilon}_r|$ and $\dot{e} = \dot{\varepsilon}_z + 2\dot{\varepsilon}_r$, with φ being the normalised shear modulus. The radial strain rate $\dot{\varepsilon}_r = 0$ owing to constraining die walls for compaction in a rigid die, giving

$$\dot{\gamma} = \left(\frac{2}{3}\right)^{1/2}|\dot{\varepsilon}_z|$$
$$\dot{e} = \dot{\varepsilon}_z \quad (14)$$

substituting equation (14) into (13), one obtains the following

$$W = \frac{1}{\rho_G^{1/2}}\left(\frac{2}{3}\varphi\dot{\varepsilon}_z^2 + \psi\dot{\varepsilon}_z^2\right)^{1/2} \Rightarrow$$
$$W = \frac{|\dot{\varepsilon}_z|}{\rho_G^{1/2}}\left(\frac{2}{3}\varphi + \psi\right)^{1/2} \quad (15)$$

combining equations (12) and (15), the axial stress is expressed as

$$\sigma_z = \frac{\sigma_y\rho_G^{1/2}}{|\dot{\varepsilon}_z|}\frac{\dot{\varepsilon}_z\left(\psi + \frac{2}{3}\varphi\right)}{\left(\psi + \frac{2}{3}\varphi\right)^{1/2}} \quad (16)$$

for compaction in a rigid die, $|\dot{\varepsilon}_z| = -\dot{\varepsilon}_z (\dot{\varepsilon}_z < 0)$. Therefore, equation (16) can be rewritten as

$$\sigma_z = -\sigma_y\rho_G^{1/2}\left(\psi + \frac{2}{3}\varphi\right)^{1/2} \quad (17)$$

the normalised shear and bulk moduli are linked to the compaction green density using Skorohod's model[49] ($\varphi = \rho_G^2$, $\psi = \frac{2}{3}\frac{\rho_G^3}{1-\rho_G}$), so substituting equation (10) into (17), it can be concluded that

$$\sigma_z = -\sigma_y\rho_G^{1/2}\left\{\frac{C}{\rho_G^{1/2}\sigma_y}\left[B - \ln\left(\frac{1-(\rho_G-\rho_A)}{\rho_A}\right)\right] + \frac{2}{3}\rho_G^2\right\}^{1/2} \quad (18)$$

for the case shown in Fig. 2, where $\sigma_z = 500$ MPa, $C = 1650$ MPa, $\sigma_y = 680$ MPa, and $B = \frac{1{\cdot}545}{D^{1/7}}$ as the rearrangement term (D is the particle size in μm), then using equation (1) leads to Fig. 3, which compares the model with experimental results for tungsten powders compacted at 240 MPa (Ref. 5). The model results are in good agreement with the experimental data. Extrapolation to a 10 nm particle size results in a low predicted green density, in agreement with early reports.[1]

Green strength

The strength of the green compact is often ignored, yet from a practical standpoint the handling strength is critical to fabrication. Routine handling requires a green strength in the 20 MPa range, but values as low as 3 MPa can be accommodated in special situations. Green strength arises from the interparticle locking, deformation, and cold welding induced by compaction. For nanoscale particles pressed at low pressures the green strength may be unacceptable, so assessment of processing viability depends on exceeding a minimum green strength. Usually green strength increases with green density, compaction pressure and particle size.[45,46,50] Data on green strength variation with particle size for tungsten[5,6] were regression fit to equation (19)

$$\sigma_G = C_1 + C_2\rho_G + C_3 D \quad (19)$$

giving the three constants as −574, 1080 and −10·7 MPa μm^{-1} respectively. This equation fits the experimental data with a statistically very significant 0·962 correlation coefficient. Figure 4 shows a plot of green strength versus particle size for a compaction pressure of 500 MPa, illustrating a lack of handling strength for compacts from particle sizes <0·2 μm or 200 nm.

Sintered density

As noted earlier, tungsten sintering has been the subject of considerable study.[1,3,5,6,20–44] Without additives to induce densification, tungsten is sintered at temperatures in the range of 1600−2500°C. The larger the particle size, the higher the required sintering temperature. In the classic treatment of initial stage sintering, shrinkage is determined by a combination of temperature T, particle size D and hold time t. The initial sintering shrinkage, $\Delta L/L_G = Y_P$, expressed as the change in green dimension divided by the green size is thermally activated[10,42,44,50]

$$Y_P = \frac{\beta t^w}{D^v}\exp\left(-\frac{Qw}{RT}\right) \quad (20)$$

where β includes material constants such as atomic

volume, atomic vibration frequency and surface energy, t is the isothermal hold time, Q is the activation energy for diffusion, T is the absolute temperature, R is the gas constant, and the exponents w and v depend on the diffusion mechanism. As sintering occurs, the microstructure scale increases owing to grain growth, so grain size G should be substituted for the particle size in equation (20). For tungsten, sintering is by a combination of surface diffusion and grain boundary diffusion,[26,28,36] but only the latter contributes to shrinkage; for pure grain boundary diffusion we would predict $w=1/3$ and $v=4/3$. However, grain growth enlarges the grain size, resulting in a slower shrinkage, while surface diffusion simultaneously consumes the sintering potential, but does not produce shrinkage. Both factors cause a considerable difference between the effective parameters in equation (20) and those expected from a single mechanism theory.[51] Data from 36 tungsten sintering experiments, referenced above, were regression fit to equation (20), giving $\beta=0{\cdot}016$, $Qw/R=4407$ K, $v=0{\cdot}33$ and $w=0{\cdot}4$ when the particle size D is in μm, temperature T is in K, and time t is in s. Since green density is determined by the particle size and compaction pressure, and sintering shrinkage is calculated from temperature and particle size, then sintered density ρ_S is determined as follows

$$\rho_S = \frac{\rho_G}{\left(1-\frac{\Delta L}{L_G}\right)^3} \tag{21}$$

sintering shrinkage is sustained only as long as the pores remain coupled with the grain boundaries.[44] In tungsten sintering, there is convergence to a steady state grain size distribution with a separation of grain boundaries from pores,[32] leading to decaying shrinkage rate versus time.[26] One consequence is that the sintering shrinkage rate declines while grain growth accelerates as pores are eliminated.[52–57] The elimination of pores results in less retarded grain growth and the grain boundaries separate from the pores, leading to stable pores and continued grain growth. Even though equation (20) predicts continued sintering shrinkage at long sintering times, measured values fall below the predictions. For tungsten, especially with a low green density, the combined roles of surface diffusion, grain boundary diffusion, grain growth and pore separation from the grain boundaries impede full densification. The implication with respect to nanoscale powders is a limited densification capacity during sintering.[53,54] These dynamics of densification and grain growth are captured by the continuum theory of sintering[48] as follows

$$\frac{d\rho_s}{dt} = \frac{9\gamma\theta}{4\eta G} \tag{22}$$

where θ is porosity, γ is the surface tension, η is the effective porous body viscosity, and G is grain size. If the density grain size behaviour is known, then equation (22) can be integrated to predict the density versus time. However, the viscosity (inversely related to the grain size and diffusion rate) must be known. The densification rate in equation (22) is coupled to grain growth, and the continuum theory of sintering gives the grain size evolution as follows[58]

$$\frac{dG}{dt} = \chi K\left(\frac{G_0}{G}\right)^{n-1}\theta^{-(n-1)/2} \tag{23}$$

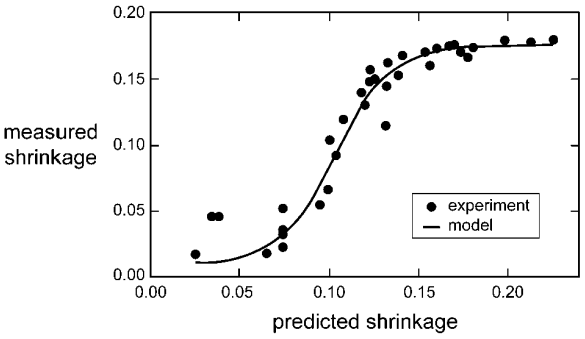

5 Sigmoid sintering shrinkage behaviour for tungsten demonstrated here using 36 experiments, showing how grain growth events late in sintering cause reduction in shrinkage

where χ is a material constant, K is the reference grain growth rate, G_0 is the initial particle size, and n is a material constant. By solving equations (22) and (23), both density and grain size can be obtained. Our fit to the sintering data referenced above give the following parameters: $\gamma=2{\cdot}65$ J m^{-2}, assuming a constant viscosity of $\eta=210\times10^{10}$ Pa s, $\chi=1{\cdot}35$, $K=1{\cdot}5\times10^{-10}$ m s^{-1} and $n=4$. This treatment shows the asymptotic character of sintering densification.

An alternative, phenomenological approach is known as the master sintering curve.[59] Here a sigmoid function is employed to incorporate the shrinkage decay behaviour associated with the shrinkage over estimation from equation (20) at higher shrinkage levels. The master sintering curve gives a parametric fit as follows

$$\left(\frac{\Delta L}{L_G}\right) = f_1 + \frac{f_2}{1+\exp\left(\frac{f_3-Y_P}{f_4}\right)} \tag{24}$$

regression analysis of the sintering data determined $f_1 = 0{\cdot}032$, $f_2 = 0{\cdot}132$, $f_3 = 0{\cdot}108$, and $f_4 = 0{\cdot}008$, using the predicted fractional shrinkage Y_P from equation (20). This equation predicts sintering shrinkage from time, temperature, and particle size with a standard error of about 1·6% shrinkage. The sigmoid characteristic is emphasised in Fig. 5. This shrinkage then allows for calculation of the sintered density using equation (21). In extreme situations the predicted density exceeds 100%, yet ρ_S is generally limited to 96% in the published data owing to grain boundary breakaway as porosity declines. Thus, an upper bound sintering density is required in those cases where intense sintering shrinkages would lead to unrealistic predicted sintering densities. The resulting predictions of sintered density versus measured density for 36 experiments are shown in Fig. 6, showing reasonable agreement with a standard error of the estimate of 3·8%.

Grain growth

As noted above, grain growth is in an inherent aspect of sintering. Likewise, grain size effects hardness, strength, and properties such as wear resistance, toughness, and ductile–brittle transition temperature. A model for final grain size in the sintered product is needed to predict properties. Equation (23) gives the instantaneous grain growth rate as a function of the porosity. An integral form is required to predict the final grain size as a function of sintering time, density and temperature. As

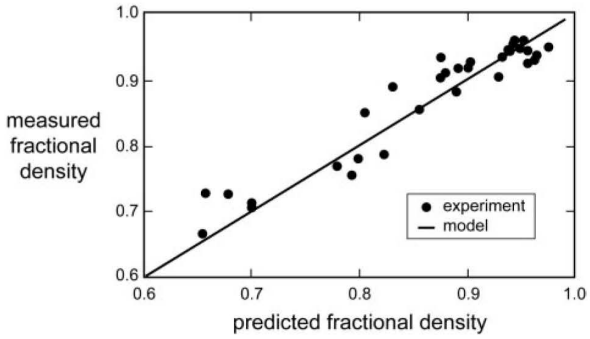

6 Comparison of experimental fractional sintered density and predicted fractional sintered density for variety of tungsten powders compacted at different pressures and sintered over range of times and temperatures

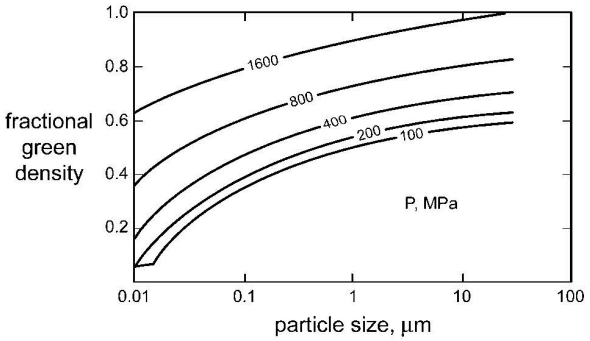

7 Model calculations of fractional green density versus particle size for various compaction pressures ranging from 1600 (top curve) to 100 MPa (bottom curve)

noted above, grain growth is inhibited early in sintering, but as pores disappear grain size enlarges rapidly.[52,54,57,60–62] Grain growth accelerates owing to fewer pore pinning sites and thermal energy is added to the system.[53,63] The grain size G after sintering can be estimated from the pore drag modified thermally activated model[44,64]

$$G = G_0 + kt^{1/3}\left(\frac{\rho_G}{1-\rho_S}\right)^{1/2}\exp\left(-\frac{Q_G}{3RT}\right) \quad (25)$$

where k is a collection of material constants, G_O is the initial grain size (assumed to be the initial particle size), t is the isothermal time at temperature T, ρ_G is the fractional green density, ρ_S is the fractional sintered density, R is the gas constant, and Q_G is the grain growth activation energy. Analysis of grain size in sintered compacts verified equation (25)[61,62] with the two constants as $k=6\ s^{-1/3}$ and $Q_G/3R=11\ 430$ K when time is in s, temperature is in K, and grain size is in μm. If the powder is highly agglomerated, the 1/2 power on the density function term tends to increase slightly.[61] For comparison, the Du–Cocks model[58] was tested against the same data, but it tended to underestimate the sintered grain size for smaller powders, making the desired extrapolations for nanoscale powders questionable.

Hardness

With the prediction of density and grain size, estimates of the sintered hardness are possible. Both density and grain size determine the hardness as well as alloying.[5,6] The hardness H for tungsten follows the Hall–Petch relation[5,6,65]

$$H = H_0 + \frac{\Theta}{G^{1/2}} \quad (26)$$

for full dense, annealed, pure tungsten the hardness ranges from 250 to 350 kg mm^{-2} depending on the grain size.[5,6,40] Impurities contribute to the hardness, so a provision needs to be added for impurity hardening. Data were collected and fit to a model that predicts hardness based on the fractional sintered density ρ_S, grain size G (in μm), and impurity content I (in ppm) as follows

$$H = \rho_S\left[H_0\left(1+\frac{I}{I_0}\right)+\frac{\Theta}{G^{1/2}}\right] \quad (27)$$

This equation was regression fit to experimental data to find $H_O=250$ kg mm^{-2}, $I_O=700$ ppm, and $\Theta=110$ kg mm^{-2} when G is measured in μm.

Strength

Although brittle at room temperature, the strength of pure tungsten at room temperature also follows a Hall–Petch dependence on grain size.[4,5] Most brittle sintered materials exhibit a linear relation between strength and hardness, with a further dependence on fractional density.[46] Lassner and Schubert[6] tabulate several determinations of room temperature strength, showing a strength as low as 180 MPa for 1 mm grain size, 400 MPa at 3·3 μm, and values in the range of 400–500 MPa for various commercial products. Regression analysis provided a model for strength σ at room temperature in MPa as a function of the hardness in kg mm^{-2} as follows

$$\sigma = 3H\rho_S^5 \quad (28)$$

where ρ_S is the fractional sintered density.

Parametric behaviour

These equations have been built from existing data and established behaviour patterns. Most of the data used to extract the parameters were taken from powders in the range of 0·3–10 μm, although data exist down to 20 nm particles. These models provide a basis for linking processing to properties based on the particle size, compaction pressure, sintering temperature, impurity level and sintering time. Other performance attributes might also be linked to these same attributes, including thermal and electrical conductivity, ductile–brittle transition temperature, wear resistance, fracture toughness and arc erosion resistance.

Property maps

Green density and strength

Figure 7 plots the fractional green density versus particle size for compaction pressures ranging from 100 to 1600 MPa. Note that at the lower pressures there is a steep increase in green density as particle size increases. Only at the higher pressures is the fractional green density for nanoscale powder comparable to that normally encountered with micrometre sized powders.

Green strength is sensitive to the compaction pressure. Smaller particles resist deformation in compaction and give a low green strength. For example, Fig. 4 plots the

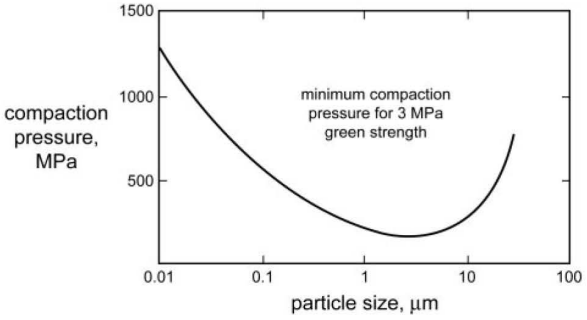

8 Calculated compaction pressures needed to generate minimum green strength of 3 MPa for range of tungsten powders: note minimum in compaction pressure in range of 1–10 μm, comparable to most standard tungsten powders

green strength versus particle size for a compaction pressure of 500 MPa. Below 100 nm there is no predicted green strength, so such powders could not be handled without the addition of polymeric binders to increase green strength. Calculations were performed to determine the minimum compaction pressure required to obtain a green strength of 3 MPa, a level deemed suitable for delicate handling. The results are plotted in Fig. 8, showing a minimum pressure for particles in the size range of 1–10 μm; higher pressures are required for nanoscale powders. About 1200 MPa would be needed for a 10 nm powder.

Sintered density and grain size

As noted above, sintered density is sensitive to the time, temperature, particle size and green density. For a 500 MPa compaction pressure and sintering for 10 h at temperatures from 1400 to 2000°C, near full density is possible for particles in the size range of 0·1–1 μm, in agreement with conventional processing. This is shown in the fractional sintered density versus particle size plot of Fig. 9. Interestingly, only at particle sizes >1 μm is there sensitivity to sintering temperature.

Figure 10 plots grain size versus particle size for the same 500 MPa compaction pressure and four sintering temperatures with a 10 h hold time. In the nanoscale particle size range a higher temperature contributed to a larger grain size, even though there was no sintered density difference. This agrees with the general finding in

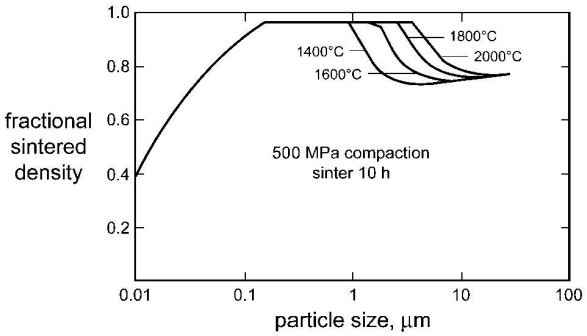

9 Predicted fractional sintered density versus particle size for tungsten powders pressed at 500 MPa and sintered for 10 h at temperatures from 1400 (lower curve) to 2000°C (upper curve)

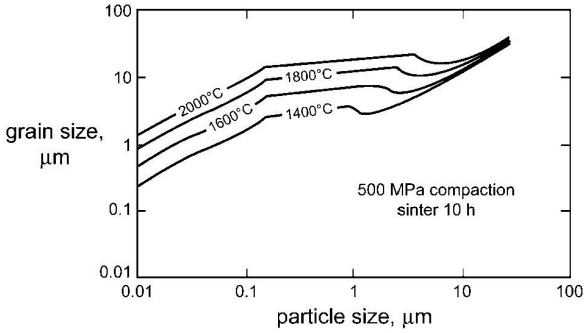

10 Plot corresponding to sintered grain size predicted for sintering temperature from 1400 (lower curve) to 2000°C (upper curve) with 500 MPa compaction pressure and 10 h sintering time

ceramics that distended green bodies coarsen, but generally fails to densify.[54]

Hardness and strength

Hardness and strength both depend on the density and grain size. The predicted hardness for 500 MPa compaction and sintering between 1400 and 2000°C for 10 h is plotted in Fig. 11. As previously noted,[5] a high hardness is possible with nanoscale grains when processed to full density. In this case, the highest predicted hardness is for a 200 nm powder sintered at the lowest temperature. The high sintering temperature is promoting grain coarsening which lowers hardness and strength. Interestingly, for 500 MPa compaction the strength peaks at a 1400°C sintering temperature and 100 nm particle size as demonstrated in Fig. 12. Over the range from 0·1 to 1 μm there is little predicted strength difference for these four sintering temperatures.

Implications

The predictions from this effort are pinned by data obtained from several different tungsten particle sizes and grain sizes. Powders used to construct the model ranged from 20 nm to 18 μm, while sintered grain sizes ranged up to nearly 100 μm. Where there are available data on sintered products, the reported properties agree with the predictions. Therefore, the model is based on reality. One significant finding is that conventional compaction pressures, which average <500 MPa, are not useful for small tungsten powders. Sintering has a

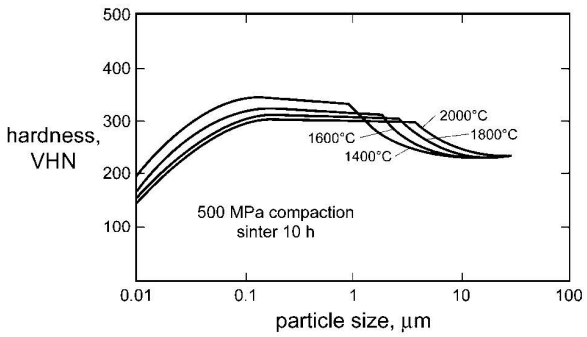

11 Plots of predicted sintered hardness versus particle size for tungsten powders compacted at 500 MPa and sintered for 10 h at temperatures from 1400 (upper curve) to 2000°C (lower curve)

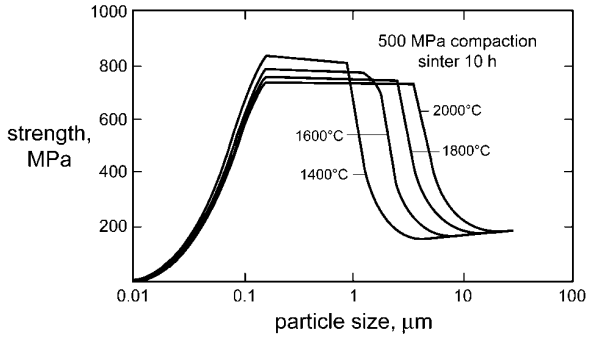

12 Predicted sintered strength for tungsten powders pressed at 500 MPa, sintered for 10 h at temperatures from 1400 to 2000°C

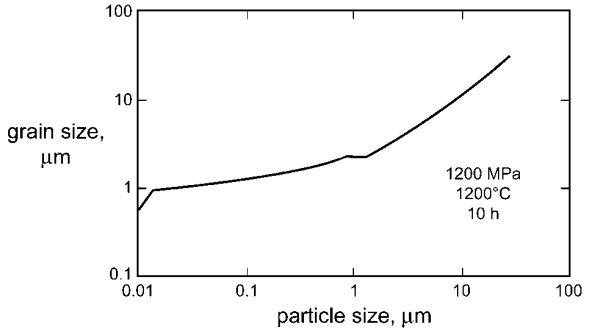

14 Predicted grain size versus particle size for tungsten powder pressed at 1200 MPa and sintered 10 h at 1200°C

limited densification potential; non-densification events such as grain growth and surface diffusion exhaust the sintering potential at low densities. Thus, compensation for the low packing densities and limited sintering densification requires very high compaction pressures. Occhionero and Holloran[61] reported less grain growth with higher green densities, and in the extreme Ahn *et al.*[66] suppressed grain growth in a nanoscale powder using a 4·5 GPa compaction pressure. Hence, there are precursor findings that support the beneficial use of high compaction pressures.

Compaction pressures near 1200 MPa are needed to induce a minimum green strength in nanoscale tungsten powders. Accordingly, calculations were performed using a constant 1200 MPa compaction pressure. The sintering cycle was set to 10 h at 1200°C with an assumed final impurity level of 100 ppm. The decision for a 1200°C temperature comes from the thermochemical analysis by Schwenke[22] and Lassner *et al.*[43] Compaction at 1200 MPa represents a constraint from the size dependent aspects of small and nanoscale tungsten powders, while the 1200°C represents a constraint from the temperature dependent aspects of tungsten. The 10 h soak was assumed since this is a typical sintering time for evaporation of impurities during tungsten sintering.[5,6]

Figure 13 shows the apparent, green and sinter densities versus particle size for this 1200 MPa and 1200°C combination. Note that high sintered densities are possible from the nanoscale powders. In parallel, calculations were performed using this same processing

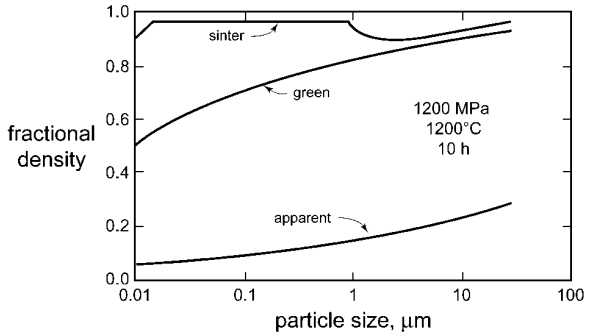

13 Fractional apparent density, green density and sintered density shown versus particle size for tungsten powder pressed at 1200 MPa and sintered 10 h at 1200°C

combination to predict the grain size in Fig. 14, and hardness and strength in Fig. 15. These plots demonstrate a high pressure, low temperature combination leading to attractive property combinations in the 100 nm particle size range. Along these lines, the strength and hardness are predicted to be nearly twice as high using small (100 nm particles) compacted at 2 to 3 GPa and sintered at 900°C for just 10 min. Gutmannas and co-workers[67,68] have previously demonstrated sintering temperature reductions with ultrahigh compaction pressures, so this scheme is reasonable using die compaction.

Other systems such as W−Cu, W−Y and W−Ni−Fe should follow similar patterns, although the powder characteristics and model parameters will differ. Extensive data exist for WC−Co over a broad range of particle sizes. Hence, similar models can be generated for these systems to allow optimisation and analysis of the impact of various combinations of processing variables.

One simple example comes with W−Cu, a system with no intersolubility. A high hardness and wear resistance are needed for applications in electrical contacts, welding electrodes and electrical discharge machining, yet the composite must be electrically conductive with sufficient tungsten to avoid arc erosion. Sintering W−Cu is identical to simply sintering the equivalent density tungsten skeleton with molten copper filling the voids between grains. Because copper does not influence the sintering,[69] the above model can be used to determine processing parameters needed to sinter an 80% dense compact with a small grain size to provide wear resistance. With 10 wt-% copper filling the pores, the composite will be fully dense with an 80% dense

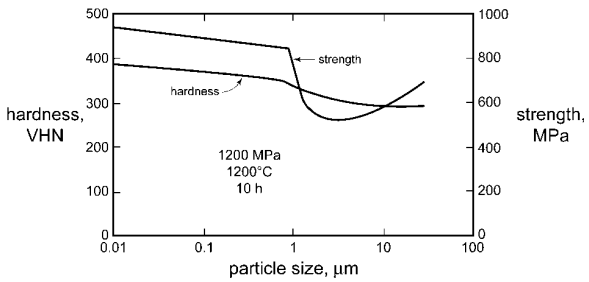

15 Sintered hardness and strength versus particle size for tungsten powder pressed at 1200 MPa and sintered 10 h at 1200°C

tungsten skeleton. Sintering must be >1100°C to remove oxygen–carbon impurities[22] and melt the copper. Based on an isothermal sintering of 60 min at 1100°C, the model shows one solution would be with a 0·16 μm powder compacted to at 1100 MPa pressure, giving a 0·81 fractional sintered density, 0·32 μm grain size, 389 HV and 384 MPa strength. For comparison, W–Cu powder with a 0·16 μm particle size and sintered with a 900–1150°C cycle produces a 0·25–1 μm grain size, 405 HV and 400 MPa strength.[10,13,19,24]

Research opportunities

Tungsten is a good choice for developing a nanoscale press–sinter model. It is an established material that is traditionally fabricated using sintering. The synthesis of nanoscale tungsten is well established by several routes.[1,70–74] Gains over many areas are anticipated from small scale microstructures, especially in electrical, mechanical and wear components. However, as shown here, new thinking is required on how to balance the size dependent advantages of small particles against inherent temperature dependent limitations. With this model, processing cycles can be optimised to better utilise nanoscale powders. High pressure compaction is indicated as a means to reduce the needed densification during sintering and concomitant grain coarsening. Clean powders will be required with such a processing scenario, because lower sintering temperatures and shorter sintering times will be less effective in evaporating contaminants. Along these lines, new research directions become evident for forming bulk structures from nanoscale powders using press–sinter techniques.

Conclusions

The present paper presents a model for the press–sinter processing of tungsten powders. The model provides insight into the interplay between the size dependent and temperature dependent processing response. It shows that features such as sintering densification and microstructure coarsening depend on both particle size and peak temperature. The model simplifies the processing, but through that simplification provides a means to effectively play out scenarios to evaluate potential gains from different particle sizes, compaction cycles, sintering temperatures, impurity levels and hold times. A few parameters dominate the processing response as well as the final strength and hardness. Other factors can be added to the predictive capability, including arc erosion resistance, thermal conductivity, electrical conductivity, ductile–brittle transition temperature, wear resistance and fracture toughness, because they depend on many of the same parameters.

The model has been used to evaluate possible processing routes to obtain improved properties from tungsten, showing that preservation of a small grain size requires significant increases in compaction pressure and decreases in sintering temperature when compared to conventional cycles. The problems with temperature dependent reactions such as oxide reduction lead to a conclusion that changes are required in powder cleanliness to avoid the microstructure coarsening concomitant with prolonged holds at high temperatures for impurity evaporation. This treatment provides insight into the processing parameter interplay as required for nanoscale powder consolidation. Opportunities arise from this model, because it greatly expedites the convergence to processing parameter combinations to deliver target properties.

Acknowledgements

This research was performed at San Diego State University during a sabbatical visit by Professor German. Supplemental financial support was provided from the Centre for Innovative Sintered Products at Penn State. The team at SDSU was supported by the National Science Foundation under Grant CMS-0301115. We are thankful to Dr D. Blaine who provided important comments on the model.

References

1. R. L. Ripley and H. Lamprey: 'Ultrafine powders', (ed. W. E. Kuhn, H. Lamprey and C. Sheer), 262–270; 1963, New York, John Wiley and Sons.
2. O. Seo, S. Kang and E. J. Lavernia: *Mater. Trans.*, 2003, **44**, 2339–2345.
3. M. I. Alymov, E. I. Maltina and Y. N. Stepanov: *Nanostr. Mater.*, 1994, **4**, 737–742.
4. E. Ivanov and E. E. Wickersham: Proc. 14th Plansee Sem., (ed. G. Kneringer, P. Rodhammer and P. Wilharitz), Vol. 1, 207–216; 1997, Reutte, Plansee AG.
5. S. W. H. Yih and C. T. Wang: 'Tungsten: sources, metallurgy, properties, and applications'; 1979, New York, Plenum Press.
6. E. Lassner and W. D. Schubert: 'Tungsten: properties, chemistry, technology of the element, alloys and chemical compounds'; 1999, New York, Kluwer Academic/Plenum Publishers.
7. E. S. Yoon, J. S. Lee, S. T. Oh and B. K. Kim: *Inter. J. Refract. Met. Hard Mater.*, 2002, **20**, 201–206.
8. G. G. Lee, G. H. Ha and B. K. Kim: *Powder Metall.*, 2002, **43**, 79–82.
9. J. S. Lee, E. S. Yoon and J. H. Yu: Proc. PM World Cong., Granada Spain, October 1998, European Powder Metallurgy Association.
10. S. S. Ryu, Y. D. Kim and I. H. Moon: *J. Alloy. Comp.*, 2002, **335**, 233–240.
11. E. S. Yoon, J. H. Yu and J. S. Lee: *J. Jpn Soc. Powder Met.*, 1999, **46**, 898–903.
12. B. K. Kim and S. H. Hong: Proc. PM World Cong., (ed. K. Kosuge and H. Nagi), 682–685; 2000, Koto, Japan, Japan Society of Powder and Powder Metallurgy.
13. I. H. Moon, S. S. Ryu and J. C. Kim: 'Sintering science and technology', (ed. R. M. German, G. L. Messing and R. G. Cornwall), 45–48; 2000, State College, Pennsylvania State University.
14. J. Fan, B. Huang, X. Qu and K. A. Khalil: *Inter. J. Powder Met.*, 2002, **38**, 56–61.
15. R. S. Biancaniello, S. D. Ridder, M. E. Williams and R. D. Jiggetts: 'Tungsten refractory metals and alloys 4', (ed. A. Bose and R. J. Dowding), 213–218; 1998, Princeton, Metal Powder Industries Federation.
16. M. N. Avettand-fenoel, R. Taillard, J. Dhers and J. Foct: *Inter. J. Refract. Met. Hard Mater.*, 2003, **21**, 205–213.
17. J. H. Yu, T. H. Kim and S. J. Lee: *Nanostr. Mater.*, 1997, **9**, 229–232.
18. I. H. Moon: 'First Japan-Korea workshop on PIM', 67–81; 1997, Pohang, Korea, Research Institute of Industrial Science and Technology.
19. J. C. Kim, S. S. Ryu, H. Lee and I. H. Moon: *Inter. J. Powder Met.*, 1999, **34**, (4), 47–55.
20. L. Bartha, P. Atato, A. L. Toth, R. Porat, S. Berger and A. Rosen: *J. Adv. Mater.*, 2000, **32**, (3), 23–26.
21. P. M. Petersson and M. Nygren: Proc. Conf. on 'Sintering', (ed. R. G. Cornwall, R. M. German and G. L. Messing); 2003, University Park, PA, Pennsylvania State University.
22. G. K. Schwenke: Proc. 15th Int. Plansee Sem., (ed. P. Rodhammer and H. Wildner),Vol. 2, 647–661; 2001, Reutte, Plansee Holding.
23. A. Updahyaya and C. Ghosh: *Powder Metall. Prog.*, 2002, **2**, 98–110.
24. D. G. Kim, E. P. Kim, Y. D. Kim and I. H. Moon: Proc. PM World Cong., (ed. K. Kosuge and H. Nagai), Part 1, 721–724;

2000, Kyoto, Japan, Japan Society of Powder and Powder Metallurgy.
25. L. P. Dorfman, D. L. Houck and M. J. Scheithauer: 'Consolidation of tungsten-coated copper composite powder', Report, Osram Sylvania, Towanda, 2002.
26. N. C. Kothari: *Powder Met.*, 1964, **7**, 251–260.
27. G. S. Upadhyaya: *Mater. Design*, 2001, **22**, 483–489.
28. M. F. Ashby: *Acta Met.*, 1974, **22**, 275–289.
29. B. R. Patterson, V. D. Parkhe and J. A. Griffin: Proc. Conf. Sintering '85, (ed. G. C. Kuczynski, D. P. Uskokovic, H. Palmour and M. M. Ristic.), 43–51; 1987, New York, Plenum Press.
30. V. V. Panichkina, V. V. Skorohod and N. P. Pavlenko: *Sov. Powder Metall. Metal Ceramic*, 1977, **16**, 950–951.
31. V. V. Skorokhod and V. V. Panichkina: Proc. PM World Cong., Granada, Spain, October 1998, European Powder Metallurgy Association.
32. B. R. Patterson, Y. Liu and J. A. Griffin: *Metall. Trans. A*, 1990, **21A**, 2137–2139.
33. R. M. German and Z. A. Munir: *High Temp. Sci.*, 1976, **8**, 267–280.
34. L. C. Chen: *Inter. J. Refract. Met. Hard Mater.*, 1994, **12**, 41–51.
35. S. Gowri and J. A. Lund: 'Tungsten and tungsten alloys – 1992', (ed. A. Bose and R. J. Dowding), 183–194; 1993, Princeton, Metal Powder Industries Federation.
36. T. Vasilos and J. T. Smith: *J. Appl. Phys.*, 1964, **35**, 215–217.
37. B. R. Patterson and V. D. Parkhe: *Prog. Powder Metall.*, 1985, **41**, 347–354.
38. R. M. German and Z. A. Munir: *Metall. Trans. A*, 1976, **7A**, 1873–1877.
39. R. D. McIntyre: *Trans. Am. Soc. Met.*, 1963, **56**, 468–476.
40. C. Selcuk, R. Bentham, N. Morley and J. V. Wood: *Inter. J. Powder Met.*, 2003, **39**, (6), 45–51.
41. A. Frisch, W. A. Kaysser and G. Petzow: 'Advances in powder metallurgy', Vol. 2, 431–444; 1989, Princeton, Metal Powder Industries Federation.
42. T. E. M. Staab, R. Krause-rehberg, B. Vetter, B. Kieback. G. Lange and P. Klimanek: *J. Phys.*, 1999, **11**, 1787–1806.
43. E. Lassner, W. D. Schubert, R. Haubner and B. Lux: 'The metallurgy of doped/non-sag tungsten', (ed. E. Pink and L. Bartha), 119–140; 1989, London, Elsevier Applied Science.
44. R. M. German: 'Sintering theory and practice'; 1996, New York, John Wiley and Sons.
45. R. M. German: 'Particle packing characteristics'; 1989, Princeton, Metal Powder Industries Federation.
46. R. M. German: 'Powder metallurgy and particulate materials processing'; 2005, Princeton, Metal Powder Industries Federation.
47. E. Olevsky and A. Maximenko: *Comp. Mater. Sci.*, 1994, **3**, 247–253.
48. E. Olevsky: *Mater. Sci. Eng. Rev. R*, 1998, **23R**, 41–100.
49. V. V. Skorohod: 'Foundations of rheological theory of sintering'; 1972, Kiev, Naukova Dumka.
50. R. M. German: *Metall. Trans. A*, 1975, **6A**, 1964.
51. R. M. German: *Powder Metall.*, 1979, **22**, 29–30.
52. I. Nettleship, R. J. Mcafee and W. S. Slaughter: *J. Amer. Ceramic Soc.*, 2002, **85**, 1954–1960.
53. J. H. Rosolowski and C. Greskovich: *J. Amer. Ceramic Soc.*, 1975, **58**, 177–182.
54. C. Greskovich and K. W. Lay: *J. Amer. Ceramic Soc.*, 1972, **55**, 142–146.
55. T. K. Gupta: *J. Amer. Ceramic Soc.*, 1972, **55**, 276–277.
56. T. K. Gupta and R. L. Coble: *J. Amer. Ceramic Soc.*, 1968, **51**, 521–525.
57. R. L. Coble and T. K. Gupta: 'Sintering and related phenomena', (ed. G. C. Kuczynski, N. A. Hooton and C. F. Gibbon), 423–441; 1967, New York, Gordon and Breach.
58. Z. Z. Du and A. C. F. Cocks: *Acta Met. Mater.*, 1992, **40**, 1969–1979.
59. H. Su and D. L. Johnson: *J. Amer. Ceramic Soc.*, 1996, **79**, 3211–3217.
60. S. C. Samanta and R. L. Coble: *J. Amer. Ceramic Soc.*, 1972, **55**, 583.
61. M. A. Occhionero and J. W. Holloran: 'Sintering and heterogeneous catalysis', (ed. G. C. Kuczynski, A. E. Miller and G. A. Sargent), 89–102; 1984, New York, Plenum Press.
62. T. S. Yeh and M. D. Sacks: *J. Amer. Ceramic Soc.*, 1988, **71**, C484.
63. T. A. Dorling and R. L. Moss: *J. Catal.*, 1966, **5**, 111–115.
64. Y. S. Kwon, Y. Wu, P. Suri and R. M. German: *Metall. Mater. Trans. A*, 2004, **35A**, 257–263.
65. V. Richter and M. V. Ruthendorf: *Inter. J. Refract. Met. Hard Mater.*, 1999, **17**, 141–152.
66. J. P. Ahn, J. K. Park and M. Y. Huh: *J. Amer. Ceramic Soc.*, 1997, **80**, 2165–2167.
67. E. Y. Gutmannas, L. I. Trusov and I. Gotman: *Nanostr. Mater.*, 1994, **4**, 893–901.
68. E. Y. Gutmanas: *Powder Met. Inter.*, 1980, **12**, 178–182.
69. J. L. Johnson and R. M. German: *Metall. Mater. Trans. B*, 1996, **27B**, 901–909.
70. E. S. Yoon, J. S. Lee and J. H. Yu: Proc. PM World Cong., (ed. K. Kosuge and H. Nagai), Part 1, 693–696; 2000, Kyoto, Japan, Japan Society of Powder and Powder Metallurgy.
71. B. H. Kim and S. H. Hong: Proc. PM World Cong., (ed. K. Kosuge and H. Nagai), Part 1, 682–685; 2000, Kyoto, Japan, Japan Society of Powder and Powder Metallurgy.
72. Y. Moriysohi, M. Futaki, S. Komatsu and T. Ishigaki: *J. Mater. Sci. Lett.*, 1997, **16**, 347–349.
73. M. H. Magnusson, K. Deppert and J. O. Malm: *J. Mater. Res.*, 2000, **15**, 1564–1569.
74. N. J. Welham: *J. Mater. Res.*, 1999, **14**, 619–627.